EFFECTS OF GREENSPACE CONFIGURATION ON THE URBAN HEAT ISLAND: A STUDY OF THE KANSAS CITY METROPOLITAN AREA

By

Elizabeth Jane Wesley

Submitted to the graduate degree program in Department of Geography and Atmospheric Sciences and the Graduate Faculty of the University of Kansas in partial fulfillment of the requirements for the degree of Master of Science in Geography.

Dr. Nathaniel Brunsell, Chairperson

Committee members

Dr. Ward Lyles

Dr. David Rahn

Date defended: April 24, 2018

The Thesis Committee for Elizabeth Jane Wesley certifies
that this is the approved version of the following thesis :

EFFECTS OF GREENSPACE CONFIGURATION
ON THE URBAN HEAT ISLAND:
A STUDY OF THE KANSAS CITY METROPOLITAN AREA

Dr. Nathaniel Brunsell, Chairperson

Date approved: April 24, 2018

Abstract

To investigate the relationship between greenspace pattern and UHIs we conducted a multi-resolution wavelet analysis of land surface temperature (LST) to determine the dominant length scales of LST. We used these scales as extents for calculating landscape metrics on a high-resolution landcover map. We built regression models to investigate whether, controlling for the percent vegetated area, patch size, fragmentation, shape, complexity, and/or proximity can mitigate UHIs. We found that more and complex patches of greenspace and dispersed rather than clustered greenspace can effectively mitigate UHIs. We also found that the negative relationship often reported between patch size and LST is an artifact of the relationship between increased percent vegetated and LST. By using the dominant length scales of LST we demonstrate that aggregation and shape complexity are important configuration factors to consider in designing urban greenspace and provide a methodology for robust biophysically-based analysis of urban landscape pattern.

Acknowledgements

I would like express my sincerest gratitude to Dr. Nathaniel Brunsell for his support, encouragement, guidance, and not least, friendship. He saw something in me that I didn't realize was there and it is my proudest accomplishment that I have become the person that he knew I was. I would also like to thank Dr. Ward Lyles for our long talks that transcended our mutual interest in sustainability and Dr. David Rahn for taking a chance on an unknown kid. Dr. Chris Brown, thank you for giving me my start. It has been a difficult and convoluted path for me to get here and I could not have done it without those who have supported me in my endeavors. I would also like to thank my supervisor at the Kansas Biological Survey, Mike Houts, for my professional start and for being so understanding about the difficulties that grad school entails. To my family and friends, thank you for your support. David Weekley and Cory Phillips, you helped me maintain my sense of humor, and Kyle Shiller, I love you.

Contents

List of Figures

List of Tables

Chapter 1

Landscape Pattern and the Urban Heat Island

1.1 Introduction

Although urban areas occupy only a small fraction of the earth's surface, they are home to more than half of the world's population, a number that is expected to increase to more than two-thirds by 2050 (United Nations, 2014). The process of urbanization is accompanied by a suite of surface modifications that alter energy flows, including the replacement of soil and vegetation with impervious surfaces like concrete and asphalt, and the emergence of a complex surface geometry resulting from buildings constructed at varying heights and densities, producing novel ecosystems whose dynamics are controlled by coupled human-natural systems (Akbari et al., 2001; Voogt & Oke, 2003; Alberti, 2010). A well-known characteristic of urban areas is an increase in temperature relative to surrounding rural areas known as the urban heat island (UHI) effect, a consequence of anthropogenic heat, decreased albedo, increased thermal capacity, and decreased evapotranspiration (Oke, 1995; Weng et al., 2008). The increase in sensible heat flux resulting from the decreased latent heat flux caused by the lack of vegetated surfaces contributes heavily to the UHI effect (Weng et al., 2004; Imhoff et al., 2010). Additionally, the increased runoff associated with impervious surfaces decreases the amount of moisture available for evapotranspiration (Grimmond & Oke, 1991). The spatial distribution of UHIs is a manifestation of the surface energy balance and is consequently strongly dependent on the presence or absence of vegetation (Weng et al., 2008; Imhoff et al., 2010), with vegetated areas being potentially 2-8°C cooler than surrounding areas (Grimmond & Oke, 1991).

Urban areas magnify the warming effects of climate change, with studies showing urban tem-

peratures to be increasing at approximately double the rate of average global warming (Stone et al., 2012). Global mean temperature is projected to warm by at least 1.5°C by the end of the 21st century and both the frequency and intensity of heat waves are expected to increase, amplifying risk for people, economies, and the environment in urban areas without sufficient infrastructure, including green-space networks (Meehl & Tebaldi, 2004; United Nations, 2014). Extreme heat events are the leading cause of weather-related mortality in the U.S. (Luber & McGeehin, 2008) and during the European heatwave of 2003, somewhere between 22,000 and 45,000 people died of heat-related illness (Patz et al., 2005). Models show that anthropogenic forcing was a significant factor in this occurrence and it is projected that the likelihood of such extreme heat events will increase 100% by 2050 (Stott et al., 2004). Urban heat directly influences air quality by facilitating the formation of ground-level ozone, a toxic gas that elevates asthma (Stone & Rodgers, 2001). Elevated temperatures also increase the use of air conditioning, thereby raising energy consumption and associated pollution levels (Synnefa et al., 2007). Urban areas are responsible for 67 - 76% of global energy consumption (Güneralp et al., 2017) and a 1996 study estimated that as much as 15% of the electricity used for cooling in Los Angeles was offsetting enhanced urban heat (Stone & Rodgers, 2001). With a greater proportion of global population living in urban areas, more people will be exposed to the risks associated with heat stress, causing not only increased mortality but also widespread economic and environmental disruption and increased energy demand (Akbari et al., 2001; Meehl & Tebaldi, 2004).

Heat island abatement is a powerful strategy to reduce heat stress and adapt to climate change (Stone & Norman, 2006) and urban planning has the potential to increase the resilience of urban areas through improvements to the built environment (IPCC, 2014). By connecting pattern to process, planners can identify thermally efficient design attributes that can be realistically applied in an urban context (Stone & Rodgers, 2001). Studies have shown that there is a strong relationship between urban land cover pattern (form) and function in urban areas (Van de Voorde et al., 2011) and it is important to understand the effects different urban forms will have on function (Alberti, 2010). If the form of an urban area can be tied to the magnitude of its UHI then effective plan-

ning and management for mitigation can occur (Stone & Rodgers, 2001; Leitao & Ahern, 2002). Landscape ecology provides a powerful paradigm for the integration of environmental science and sustainability through the design of the built environment (Wu, 2010) and the tools necessary to characterize the urban environment and quantitatively relate it to biophysical processes (Weng et al., 2008). To understand how urbanization patterns affect ecosystem dynamics, common metrics are necessary (Alberti, 2010). Landscape metrics are indices that were created by landscape ecologists to quantify the pattern of land cover within a landscape based on the fundamental idea that environmental patterns influence ecological processes (McGarigal, 2014). Landscape metrics are especially well suited to describing urban areas because the basic land-cover classes are well defined and the landscape structure is fairly static; they can also facilitate information exchange between scientists and planners by providing a language common across these disciplines (Leitao & Ahern, 2002).

UHIs can be potentially reversed by greening urban areas (Streutker, 2002). Urban greenspace has a consistently positive effect on UHI mitigation (Buyantuyev & Wu, 2010; Li et al., 2011; Maimaitiyiming et al., 2014) and vegetated cover and impervious surface are the two most important factors in UHI formation (Huang et al., 2011). The pattern of urban greenspace influences the distribution and magnitude of land surface temperatures (LST) through its effects on energy flows in urban areas (Zhou et al., 2011; Maimaitiyiming et al., 2014) and can be controlled through urban planning (Weng et al., 2007). Pattern comprises composition, the variety and abundance of landcover types, and configuration, their arrangement and distribution (McGarigal, 2014). Urban greenspace composition, i.e. the percent vegetated cover, has been repeatedly shown to mitigate UHIs (Weng et al., 2004; Yuan & Bauer, 2007; Li et al., 2011; Chen & Yu, 2017), however, the effects of greenspace configuration, especially when controlling for the effects of composition, are more complicated and less well understood (Zhou et al., 2011). Li et al. (2011) found that given a set quantity of greenspace, dispersed rather than concentrated configurations more effectively mitigate UHIs. Likewise, Stone and Rodgers (2001) found that dispersed rather than clustered distributions of neighborhood street trees can more significantly influence LSTs than the total number

of trees. Zhou et al. (2011) reported negative relationships between LST and edge density and shape complexity and no significant relationship between mean patch size and LST. More recently, Li et al. (2016) found that configuration had a stronger correlation with LST than composition. Li et al. (2012) and Chen & Yu (2017) found that larger vegetated patches more effectively lowered LST. In contrast to Li et al. (2011) and Stone & Rodgers (2001), Chen & Yu (2017) and Estoque et al. (2017) found that aggregated rather than dispersed greenspace more effectively lowered LST.

There has been recent interest in relating the configuration of urban greenspace to UHIs using landscape metrics (Zhou et al., 2011; Li et al., 2011, 2012; Maimaitiyiming et al., 2014; Li et al., 2016; Chen & Yu, 2017; Estoque et al., 2017), however there are still knowledge gaps. When calculating landscape metrics the scale at which they are calculated must represent the biophysical process under consideration or the results are essentially meaningless (McGarigal, 2014). The characteristic scale of a phenomenon is the scale at which it predominantly operates and if it is not matched by the scale of observation the phenomenon may be not be properly observed (Wu, 2007). The complexity of urban environments increases the difficulty of modeling the relationship between structure and function (Weng et al., 2008; Alberti, 2010; Grafius et al., 2018) and care must be taken to do so at relevant scales. In several of these studies the scale at which landscape metrics were calculated to compare greenspace configuration with LST were census tracts (Li et al., 2012, 2016) whose borders have little to do with microclimatic interactions, with Li et al. (2016) using only a sample of census tracts that were primarily single-family residential. Zhou et al. (2011), Chen & Yu (2017), and Grafius et al. (2018) calculated metrics for variably-sized patches based on urban land heterogeneity, the standard deviation of LST, and urban land-cover classes respectively. However, comparison of landscape pattern must be based on the same extent to be meaningful (Wu, 2004). While Li et al. (2011) calculated metrics within 2 km extents, Maimaitiyiming et al. (2014) within a 500 m moving extent, and Estoque et al. (2017) within 3 km extents, none of these studies give biophysical justification for their choice of extent. Furthermore, the maximum number of dates for which the UHI was examined in any of these studies was two (Li et al., 2011). Accordingly, Zhou et al. (2011) and Li et al. (2016) call for future studies to use

multiple images to account for variance in local and regional weather patterns (Kim & Baik, 2005). Increasing the temporal extent of LST observations will also provide for more robust statistical results (Hu & Brunsell, 2015). The purpose of this study is to examine the relationship between urban greenspace configuration and LST at relevant spatial scales while controlling for the percent vegetated cover. By quantifying landscape pattern at the characteristic scales of vegetation-LST interaction we can determine which elements of landscape pattern are biophysically relevant to mitigation of the UHI in the Kansas City metropolitan area.

1.2 Data

1.2.1 Study Extent

The Kansas City metropolitan area is located at 39.0398°N latitude and 94.5949°W longitude and spans two states and six counties: Johnson and Wyandotte Counties in Kansas, and Platte, Clay, Cass, and Jackson Counties in Missouri. The Kansas City, MO - KS urbanized area as delineated by the United States Census Bureau had a population of 1,519,417 in 2010, an estimated 8% increase from 2000 (U.S. Census Bureau, 2010). The Köppen climate classification is humid subtropical (Cfa), with annual average rainfall of 964 mm (https://en.climate-data.org/location/715044). The greater Kansas City area is located in the Great Plains Level I Ecoregion, the Temperate Prairies Level II Ecoregion, and straddles the Central Irregular Plains and the Western Corn Belt Plains Level III Ecoregions (https://www.epa.gov/eco-research/ecoregions). The Kansas City metropolitan area exhibits patterns of urban sprawl, which is generally defined as "geographic expansion over large areas, low-density land use, low land-use mix, low connectivity, and heavy reliance on automobiles relative to other modes of travel" (Fig. 1.1) (Stone et al., 2010); indeed, Ji (2008) found that for the larger Kansas City Metropolitan Statistical Area there was a 55 percent increase in built area between 1972 and 2001. These patterns of development and the subsequent fragmentation of greenspace are likely to have significant effects on spatial patterns of temperature (Stone & Norman, 2006).

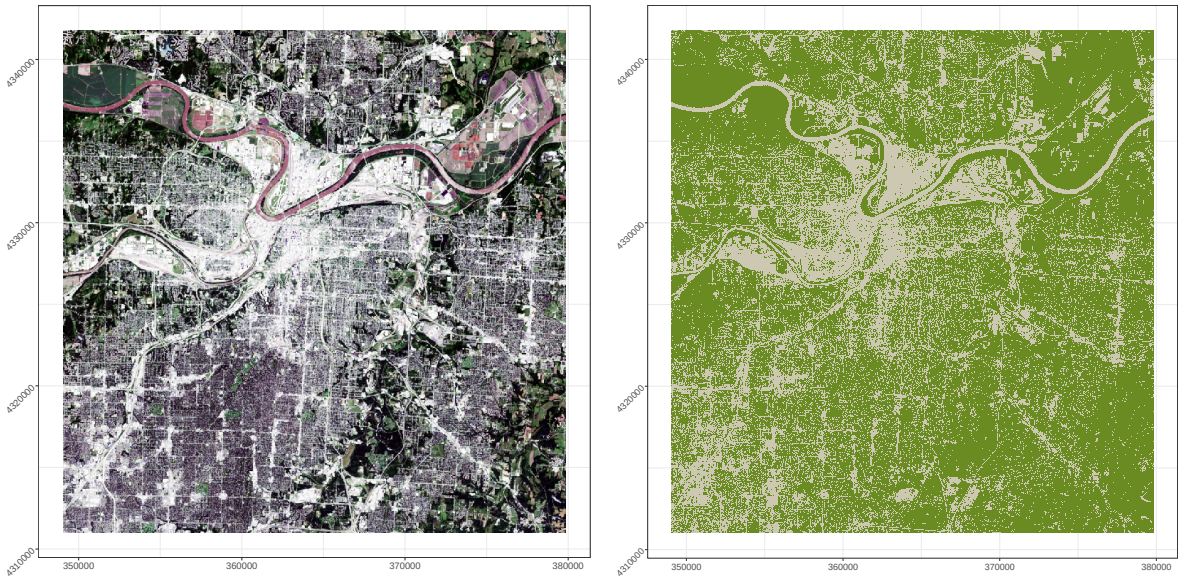

Figure 1.1: Study extent of the Kansas City metropolitan area with the binary land-cover raster on the right. Green represents vegetated surfaces and grey represents non-vegetated surfaces.

1.2.2 Landcover

We used a high-spatial resolution (2.5 m) land cover map for the calculation of landscape metrics. The Mid-America Regional Council (MARC) created the Natural Resources Inventory (NRI) map of Greater Kansas City with an object-based classification, using SPOT data from May, June, and August of 2012 as well as ancillary data (LiDAR, hydrography, parcels/zoning class, transportation centerlines, streamlines, and floodplains). The resulting land cover map has an estimated accuracy of 83 - 91% for the Level I classifications of impervious, barren, vegetated, and water. Impervious comprises buildings and other impervious surfaces, barren comprises land with 0 - 10% vegetated fraction, vegetated comprises land with 10-100% vegetated fraction, and water comprises water features. The spatial resolution of the NRI landcover map is 2.5 m and the extent is the 4,423 square miles that comprise the 9 county Kansas City metropolitan area (Mid-America Regional Council, 2013). We further classified the landcover to produce a binary raster consisting of vegetated and non-vegetated (impervious, barren, water) pixels (Fig. 1.1).

1.2.3 Landsat

We processed Landsat data into both fractional vegetation cover (Fr) and LST. LST is the result of surface-atmosphere interactions and energy fluxes that vary with landcover, and is an important parameter for examining UHIs (Liu & Weng, 2009). Landsat is the most frequently used medium-resolution imagery for UHI studies (Li et al., 2013) and is free and readily available. Due to the scan corrector failure of Landsat 7 and Kansas City's location along the edge of the Landsat scenes that cover the metropolitan area, data from 2012 suffered from considerable data loss. Instead, we used the Level 1 precision terrain corrected scenes from Landsat 5 in 2011 and Landsat 8 in 2013, operating under the assumption that there was minimal change in land cover classes between these years. Only primarily cloud-free images were used, resulting in five suitable images from 2011 (June 7, July 2, July 18, July 25, August 19) and one from 2013 (June 28). The summer of 2011 had a June-July-August average maximum temperature of 34.38°C which is significantly higher than the 2013 average of 30.55°C (www.ncdc.noaa.gov/cdo-web/datasets). Each scene was clipped to the study extent.

We calculated Fr from the Normalized Difference Vegetative Index (NDVI) which is related to the density of green leaves in a pixel and is defined as:

$$NDVI = \frac{\rho_{NIR} - \rho_{red}}{\rho_{NIR} + \rho_{red}} \tag{1.1}$$

where ρ_{NIR} and ρ_{red} are the surface reflectance values in the near-infrared and red bands, respectively. Fr is the vegetated proportion of a pixel and is defined as:

$$Fr = \left(\frac{NDVI - NDVI_{soil}}{NDVI_{veg} - NDVI_{soil}} \right)^2 \tag{1.2}$$

where $NDVI_{soil}$ and $NDVI_{veg}$ are the NDVI values corresponding to bare soil and fully vegetated pixels, respectively (Gillies & Carlson, 1995). These values were chosen based on manual examination of each image. All NDVI values less than $NDVI_{soil}$ in a given image were set to NA and

all Fr values greater than 1 were set to 1. A mask was created to exclude all water pixels using the Modified Normalized Difference Water Index proposed by Xu (2006) and given as:

$$MNDWI = \frac{\rho_{green} - \rho_{SWIR}}{\rho_{green} + \rho_{SWIR}} \tag{1.3}$$

where ρ_{green} and ρ_{SWIR} are the surface reflectance values in the green and shortwave infrared bands, respectively. The MNDWI of the Landsat 5 image from June 7, 2011 provided the most accurate water mask with the least noise and was used for all the Landsat scenes with the assumption that there was little change in water bodies between 2011 and 2013. The Fr of all water pixels was set to 0.

The top of the atmosphere radiance was calculated according to the methods provided in the Landsat 8 (L8) Users Handbook (U.S. Geological U.S. Geological Survey, 2016). Per pixel emissivity values were calculated according to Brunsell and Gillies (2002) with

$$\varepsilon = Fr * \varepsilon_{veg} + (1 - Fr) * \varepsilon_{urb} \tag{1.4}$$

where ε_{veg} is the emissivity of a fully vegetated pixel and ε_{urb} is the emissivity of a pixel covered by impervious surface. These values were defined as 0.96 and 0.88 respectively based on (Zhou et al., 2014). We then calculated the total radiant heat energy assuming an emissivity of 1 according to the Stefan-Boltzman equation, $L = \sigma T^4$, where σ is the Stefan-Boltzman constant and T is temperature in Kelvin. LST was then calculated by scaling the calculated radiant heat energy by the calculated emissivity

$$LST = \sqrt[4]{\frac{L}{\varepsilon * \sigma}} \tag{1.5}$$

where L is the radiant heat energy, ε is the emissivity, and σ is the Stefan-Boltzman constant, and then adjusting to degrees Celsius. The QA band of the Landsat data was used to mask any cloud interference using both the cloud and cloud shadow rasters. All pixels designated as clouds were assigned to NA values.

1.3 Methodology

1.3.1 Multi-resolution Wavelet Analysis of LST

Identifying the characteristic scales of pattern and process is critical for understanding phenomena and the scale of analysis should reflect this process scale. Urbanization is a multi-scale process and therefore requires multi-scale information to observe relevant patterns (Wu, 2004, 2007; Buyantuyev et al., 2010). Wavelet analysis is an inherently multi-scaled method for identifying the characteristic scales of landscape structure (Wu, 2004). Wavelet transforms provide the ability to examine variability across scales and to determine which scale contributes most to the variability of a signal (Brunsell & Gillies, 2003). The dominant length scale is the scale at which wavelet variance is greatest and provides information about the scales at which features make significant contributions to the signal (Kumar & Foufoula-Georgiou, 1997). We conducted a multi-resolution wavelet analysis to determine the dominant length scales of LST in the study area. The dominant length scales of LST provide information about the scale at which biophysical interactions on the Earth's surface produce temperature.

Wavelet analysis does not work well with NA values, so any pixels with a value of NA were set to the mean LST of the study area on that date. Then we conducted a multi-resolution wavelet analysis using the waveslim package in R by performing a nine-level additive decomposition using the pyramid algorithm, where the pixel values of the image at a given scale are the sum of the horizontal, vertical, and diagonal directions and represent the contribution of that scale to the variance of LST on that date (Fig. 1.2) (Whitcher, 2014). We took the scale with the maximum contribution to the variance for each pixel as the dominant length scale for the pixel. If there was more than one maximum value, we chose the lesser of the scales.

1.3.2 Calculation of Landscape Metrics

The dominant length scale of each pixel represents the spatial scale at which the LST at that pixel was produced. This is the extent within which we calculated landscape metrics to investigate the

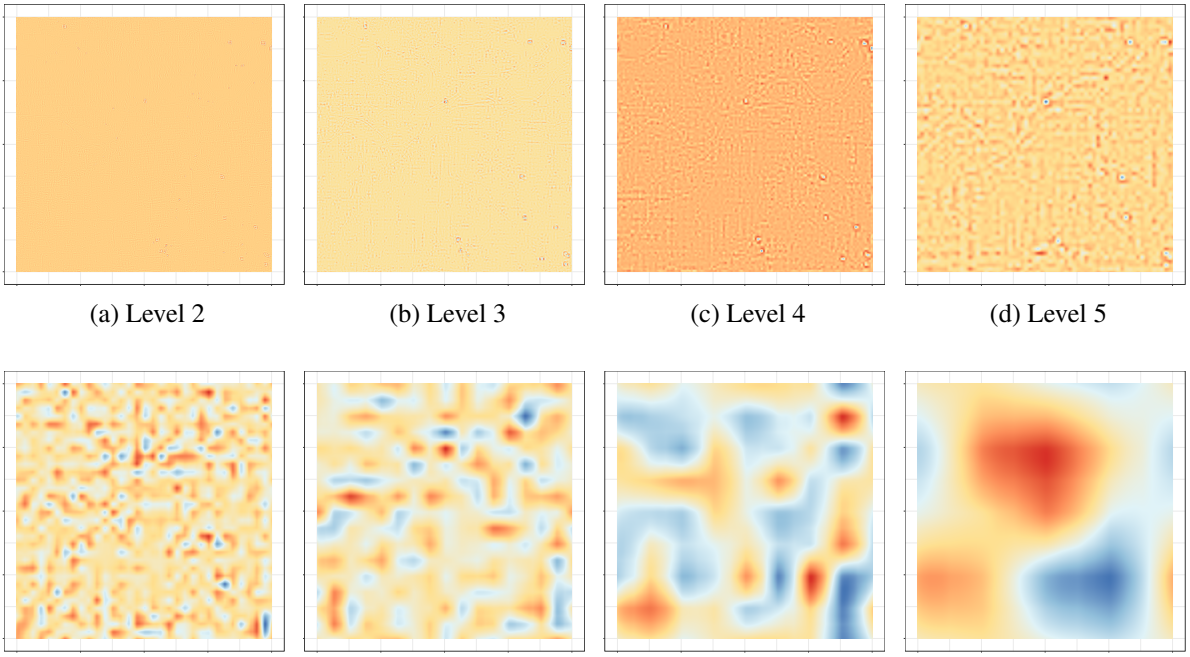

(a) Level 2 (b) Level 3 (c) Level 4 (d) Level 5

(e) Level 6 (f) Level 7 (g) Level 8 (h) Level 9

Figure 1.2: Wavelet coefficients for the nine level multi-resolution decomposition from July 2, 2011. Level one is not included.

relationship between LST and landscape configuration at the operational scale of vegetation-LST interaction. The calculation of landscape metrics was temporally and computationally expensive so we conducted the analysis for a sample of pixels at each dominant length scale, for each date. We originally calculated the dominant length scale for ten levels. However, the time required for calculating the landscape metrics increased exponentially as the extent resolution increased. The dominant length scale of ten corresponds to a resolution of 30,720 m and the sample of 100 for each of six dates would have taken over six months to complete. Consequently we recalculated the dominant length scales for nine levels and selected all of the sample pixels whose dominant length scale was the same for both nine and ten levels. Although this resulted in an unequal number of samples per scale and date (Table 1.1), the subsequent analysis removed the effects of scale and date from the models. Each sampled pixel was transformed to its centroid and the LST extracted to it; a square buffer whose extent corresponds to the resolution of the dominant length scale was then centered on the point. Landscape metrics (Table 1.2) were calculated within this extent on

	2	3	4	5	6	7	8	9
June 7, 2011	33	157	103	46	173	151	57	11
July 2, 2011	43	145	89	41	192	172	81	41
July 18, 2011	42	129	87	28	140	152	57	20
July 25, 2011	43	147	85	31	130	150	61	34
August 19, 2011	52	149	80	30	144	129	39	30
June 28, 2013	48	143	45	39	39	34	148	28
Total	261	870	489	215	818	788	443	164

Table 1.1: Sample size for each date and dominant length scale.

Pattern Measure	Landscape Metric
Composition	Proportion of Landscape
Patch Size	Patch Size Distribution
Fragmentation	Largest Patch Index Patch Density Total Edge Edge Density
Shape	Shape Index Distribution
Connectivity	Patch Cohesion Index
Proximity	Proportion of Like Adjacencies

Table 1.2: Calculated landscape metrics

the binary land cover raster for the vegetated surfaces, using the spatialEco package in R. These metrics are considered class-level metrics because they describe the pattern of a landcover class within each extent rather than describing each individual patch within an extent (McGarigal, 2014).

Landscape metrics were chosen to reduce redundancy while providing a full description of landscape configuration, with an emphasis on metrics that have practical urban planning applications. Following the work of Zhou et al. (2011) and Leitao & Ahern (2002), the metrics in Table 1.2 were selected. All of these metrics are simple to implement in an urban design context and are easy to comprehend. Composition measures the amount of greenspace in an area; patch size measures how large each patch of greenspace is; fragmentation and connectivity measure how connected these patches of greenspace are; shape is a measure of the complexity of the shapes of the greenspace patches; and proximity measures how close the patches are to each other.

Composition refers to the amount of a vegetated surfaces within an area and is measured by the

proportion of the landscape composed of vegetated surfaces and calculated as:

$$PLAND = \frac{\sum_{j=1}^{n_i} a_{ij}}{A}(100) \tag{1.6}$$

where n_i is the number of vegetated patches, a_{ij} is the area (m^2) of patch ij, and A is the total area (m^2) of the extent (McGarigal, 2014). This was used to control for the effects of the percent of vegetated cover which strongly influences LST (Weng et al., 2004; Yuan & Bauer, 2007; Li et al., 2011; Hu & Brunsell, 2015). Configuration refers to the pattern of a land cover type within an area and was measured with a combination of patch size, fragmentation, shape, and connectivity metrics. Patch size was measured by:

$$AREA = a_{ij} \tag{1.7}$$

where a_{ij} is the area (m^2) of patch ij. The statistical distribution of vegetated patch sizes, including the mean, minimum, maximum, and standard deviation, were calculated for each dominant length scale extent. The degree of fragmentation was measured with three metrics: the largest patch index, the patch density, and the edge density. The largest patch index is the percentage of each dominant length scale extent comprised of the largest vegetated patch

$$LPI = \frac{max_{j=1}^{n}(a_{ij})}{A}(100) \tag{1.8}$$

where $max_{j=1}^{n}(a_{ij})$ is the maximum patch size within the extent and A is the total area (m^2) of the extent. LPI will be one if the extent is comprised of only a single vegetated patch and near zero if there are very few vegetated patches. The patch density is the number of vegetated patches divided by the area of the extent

$$PD = \frac{n_i}{A} \tag{1.9}$$

and will reach increase with the number of vegetated patches. A high PD is an indicator of disaggregation of greenspace. The total edge is the total perimeter length of all vegetated patches within

an extent,

$$TE = \sum_{k=1}^{m} e_{ik} \tag{1.10}$$

where e_{ik} is the total perimeter length of the vegetated patches. The edge density is the total perimeter length of all vegetated patches within an extent divided by the area of that extent,

$$ED = \frac{\sum_{k=1}^{m} e_{ik}}{A} \tag{1.11}$$

where e_{ik} is the total perimeter length of the vegetated patches. The shape of the vegetated patches is quantified by the statistical distribution of the shape index which provides a standardized measure of shape complexity calculated from the perimeters of the vegetated patches within each extent,

$$SHAPE = \frac{P_{ij}}{min_{P_{ij}}} \tag{1.12}$$

where P_{ij} is the perimeter of patch ij and $min_{P_{ij}}$ is the minimum vegetated patch perimeter within the extent of the dominant length scale. SHAPE is a measure of disaggregation. Connectivity was measured with the patch cohesion index which is a measure of the physical connectedness of the vegetated patches within each dominant length scale extent,

$$COHESION = \left[1 - \frac{\sum_{j=1}^{n} P_{ij}}{\sum_{j=1}^{n} P_{ij}\sqrt{a_{ij}}}\right]\left[1 - \frac{1}{\sqrt{A}}\right]^{-1}(100) \tag{1.13}$$

where P_{ij} is the perimeter of patch ij, a_{ij} is the patch area (m^2) , and A is the total area (m^2) of the extent. The patch cohesion index increases as patches become more aggregated. Finally, the proximity of vegetated patches to each other was measured by the proportion of like adjacencies, which measures the degree of aggregation of vegetated patches and is calculated by

$$PLADJ = \left(\frac{g_{ij}}{\sum_{k=1}^{m} g_{ik}}\right)(100) \tag{1.14}$$

where g_{ii} is the number of like adjacencies between vegetated pixels and g_{ik} is the total number of

adjacencies for vegetated pixels (McGarigal, 2014; Evans, 2017). Both minimum patch size and minimum shape index were removed from the analysis because of the large number of redundant values.

1.4 Results

1.4.1 Variation across scale and percent vegetated class

We completed the multi-resolution wavelet analysis and subsequent metric calculations for a sample of each dominant length scale for each of the six dates (Fig. 1.3). The dominant length scales gave us the extent within which the metrics were calculated and represent the characteristic scales of vegetation-LST interactions. The dominant lengths scales followed approximately the same distribution for each date although July 2 and July 25 both peaked in the high scales rather than the middle scales (Fig. 1.4). These dates also had the highest temperatures. Although the LSTs for each date followed approximately the same distribution, August 19, 2011 had lower temperatures (Fig. 1.5). LST anomalies were calculated by subtracting the median temperature by date from each LST observation to facilitate comparison across the six dates. From now on when referring to LST we are referring to the LST anomaly unless otherwise noted. For June 6, June 28, July 18, and July 19, the mid-dominant length scales correspond to the highest temperatures. July 2 and July 25 have the highest temperatures at the high scales.

1.4.1.1 LST Variation

LST varied with both scale and percent vegetated. LSTs were lowest for scales two and three and then approximately the same for scales 4 through 8, with most dates showing a slight increase for scale nine (Fig. 1.6a). LST also varies fairly predictably with percent vegetated, with areas with a higher percent of greenspace cover showing lower temperatures at any given scale (Fig. 1.6b). It is worth noting that as scale increases, both the lowest and highest vegetated classes drop out. The larger the area, the more likely it is that there will be some amount of greenspace and the less

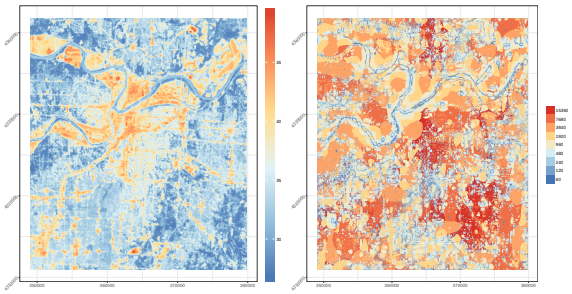

(a) LT5 June 7, 2011

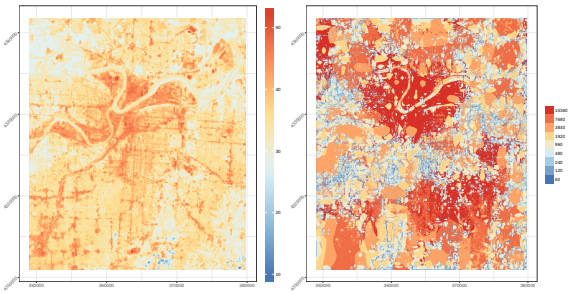

(b) LT5 July 2, 2011

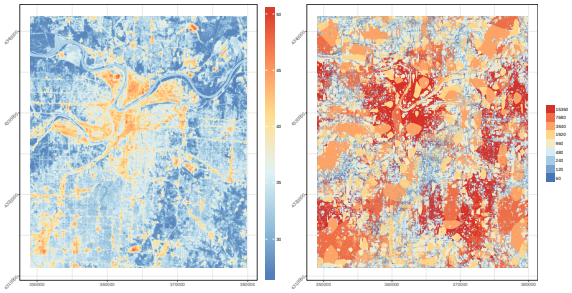

(c) LT5 July 18, 2011

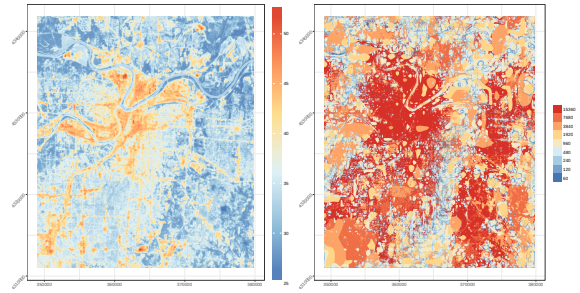

(d) LT5 July 25, 2011

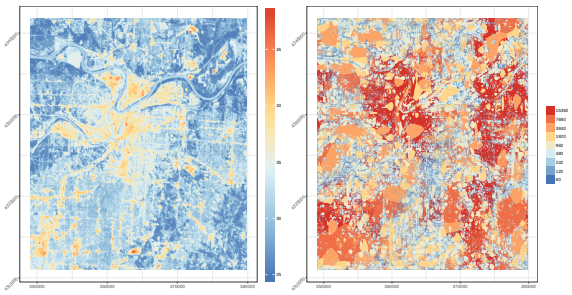

(e) LT5 August 19, 2011

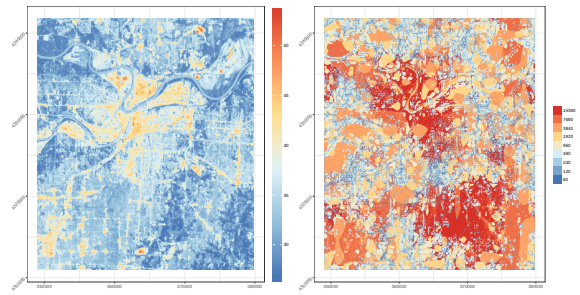

(f) LC8 June 28, 2013

Figure 1.3: LST and dominant length scales for the Landsat scenes. LST in degrees C are on the left and the dominant length scale is on the right.

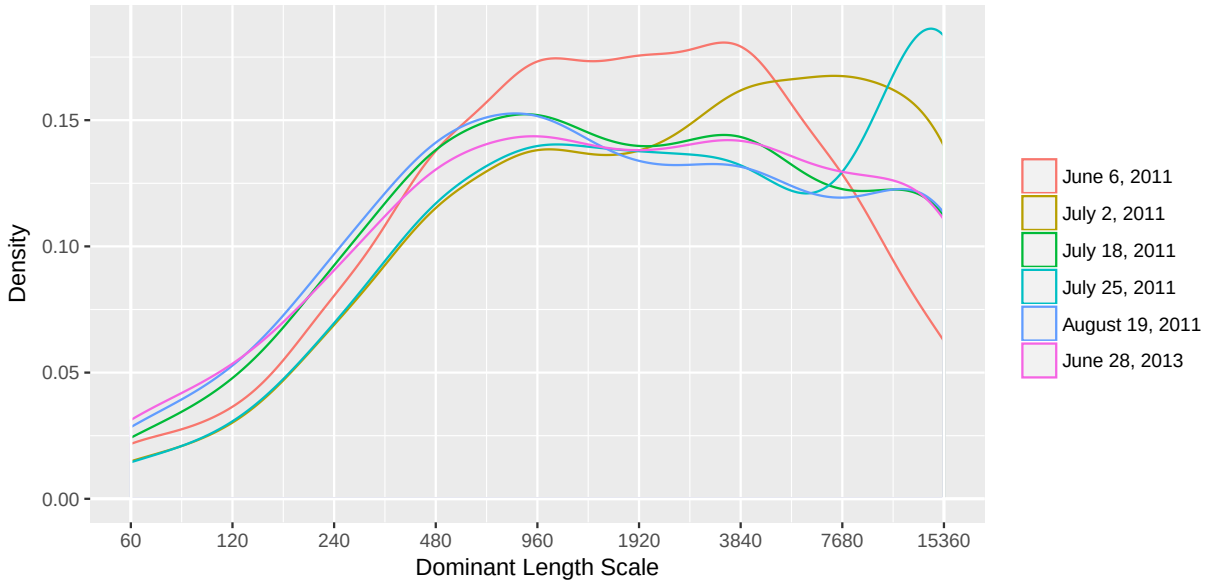

Figure 1.4: Distribution of dominant length scale by date.

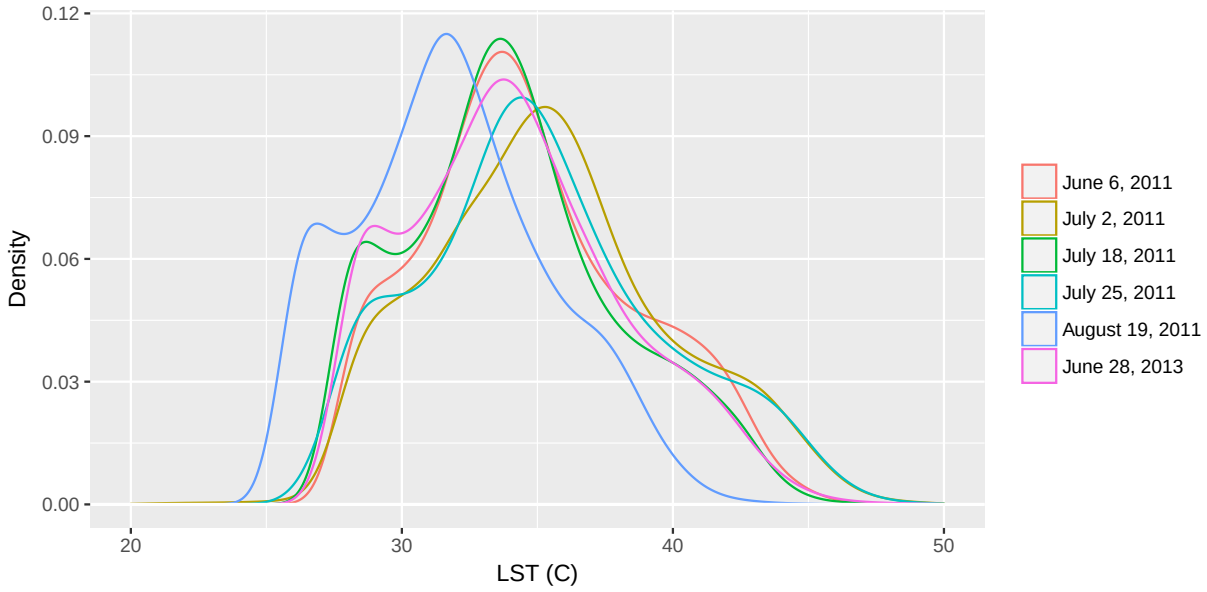

Figure 1.5: LST distribution by date.

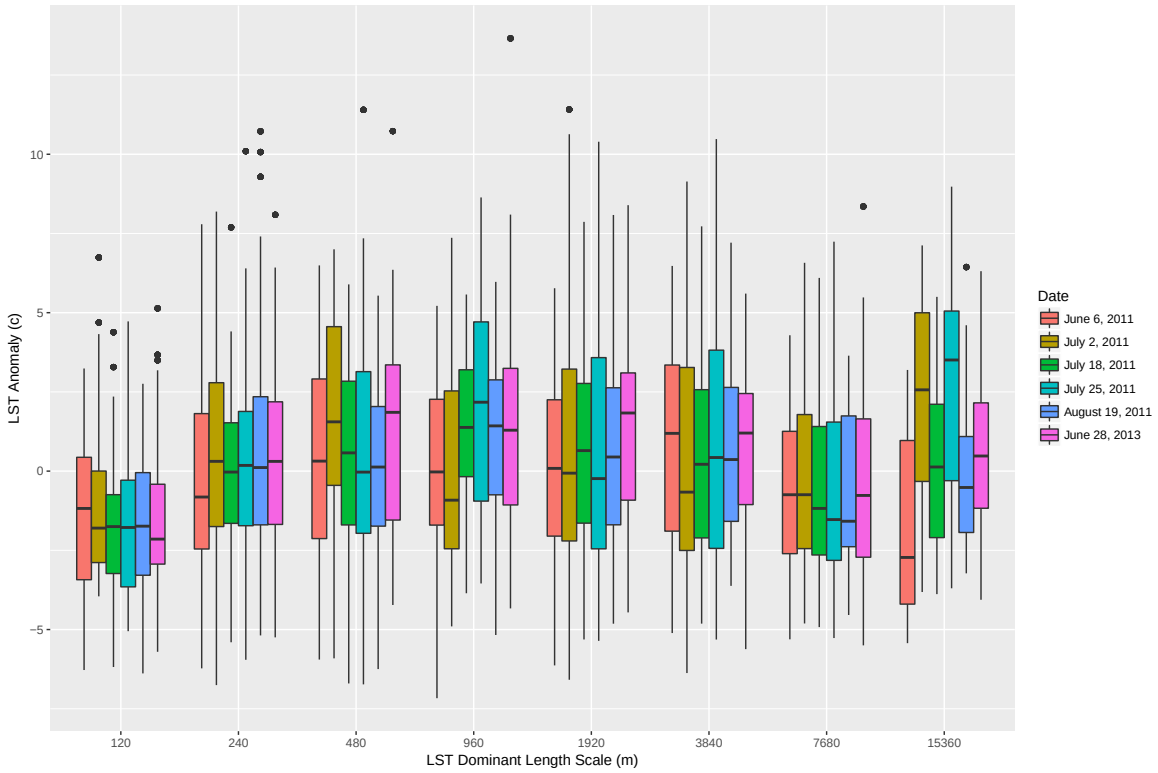

(a) By dominant length scale.

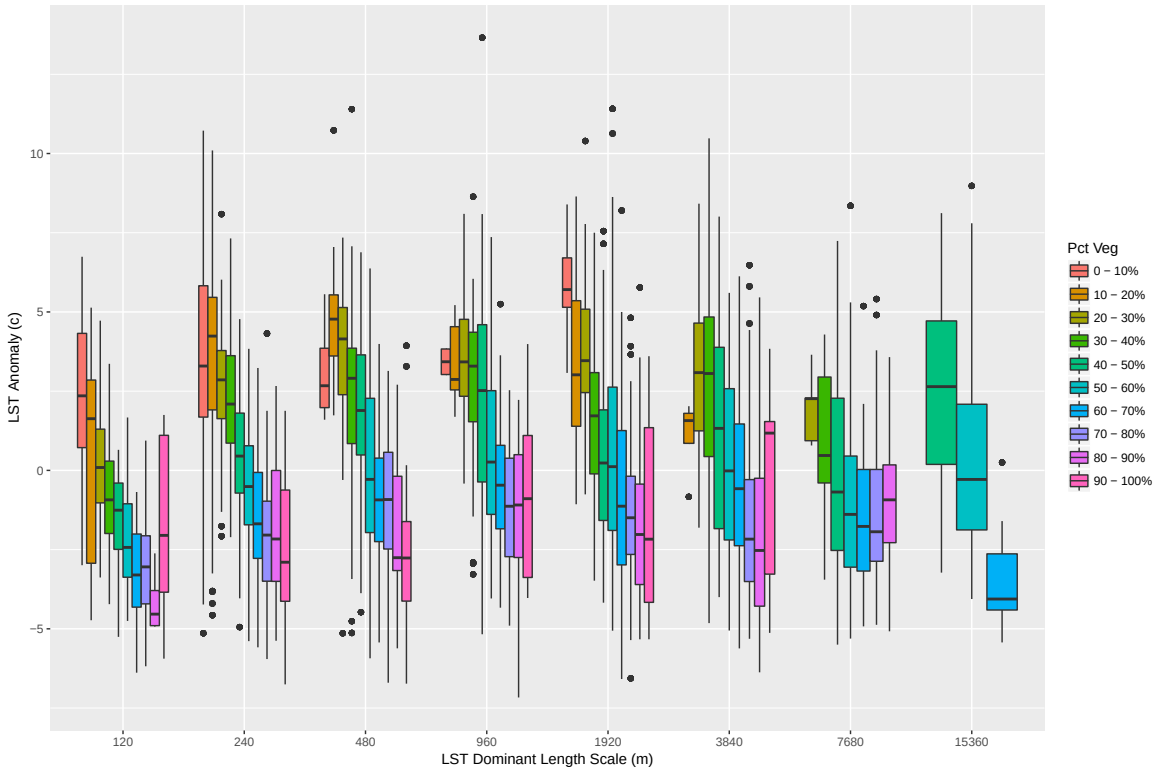

(b) By percent vegetated class

Figure 1.6: LST anomalies

	LST Scale	Pct. Veg.
Patch Density	-0.37	-0.34
Total Edge	0.98	0.19
Edge Density	-0.24	0.18
Largest Patch Index	-0.68	0.41
Mean Patch Area	0.35	0.70
Std. Dev. of Patch Area	0.66	0.61
Max. Patch Area	0.91	0.44
Mean Shape Index	0.24	0.23
Std. Dev. of Shape Index	0.57	0.22
Max. Shape Index	0.91	0.17
Proportion of Like Adjacencies	0.38	0.70
Patch Cohesion Index	0.76	0.50

Table 1.3: Correlations between metrics and dominant length scale and percent vegetated. All values are significant at the 0.001 level.

likely it is that the area will be a majority greenspace. This is also a consequence of the wavelet analysis; eventually the coarsest scale of decomposition will approach a constant value which is the mean LST. This indicates that the areas with the highest and lowest percent vegetated do not make significant contributions to mean LST.

1.4.1.2 Metric Variation

The landscape metrics also varied with both scale and percent vegetated. All of the metrics showed consistent scaling relations with increasing extent although some were more robust than others (Fig. 1.7). With log-transformation, total edge, largest patch index, maximum patch area, and maximum shape index all showed linear relationships with scale while the remaining metrics all showed either logarithmic or inverse logarithmic relationships. All the metrics were significantly correlated with scale (Table 1.3). This is part and parcel of the modifiable areal unit problem that plagues most geographic analysis as each scale is a dyadic increase in area of the extent.

Comparison of landscape pattern must be based on the same extent (Wu, 2004); to allow comparison of metric values across dominant length scale extents, linear regressions were fit between each metric and the resolution at each scale (Table 1.4) and the best fit models were chosen by their R^2 values. In order to remove the impacts of scale, we calculated the residuals from these

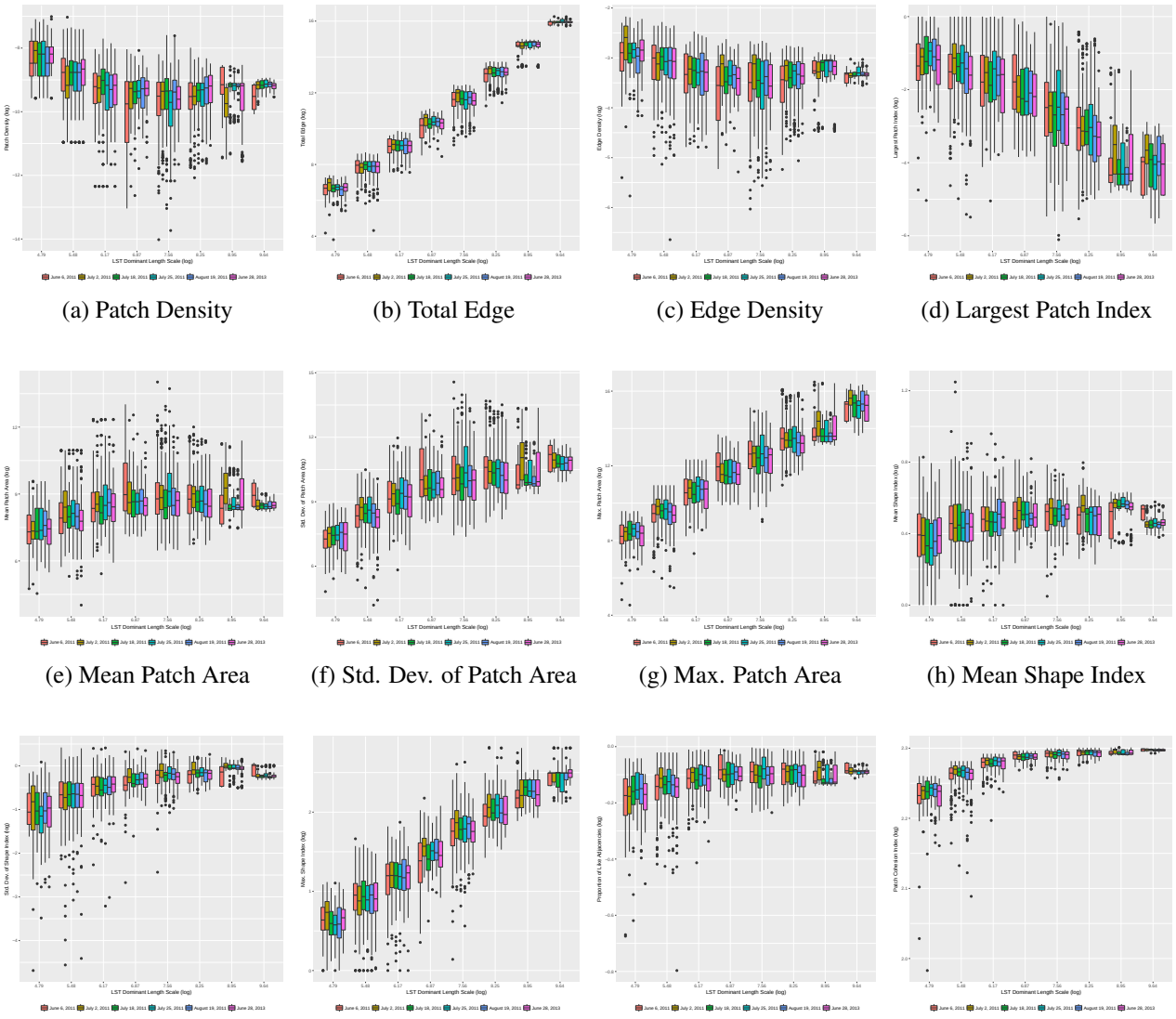

(a) Patch Density (b) Total Edge (c) Edge Density (d) Largest Patch Index

(e) Mean Patch Area (f) Std. Dev. of Patch Area (g) Max. Patch Area (h) Mean Shape Index

(i) Std. Dev. of Shape Index (j) Max. Shape Index (k) Prop. Like Adjacencies (l) Patch Cohesion Index

Figure 1.7: All landscape metrics showed consistent scaling relations although some were more robust than others.

	Metric	Model	R^2
1	Patch Density	y ~ log(x)	0.18
2	Total Edge	log(y) ~ log(x)	0.97
3	Edge Density	y ~ log(x)	0.09
4	Largest Patch Index	y ~ log(x)	0.29
5	Mean Patch Area	log(y) ~ log(x)	0.09
6	Std. Dev. of Patch Area	log(y) ~ log(x)	0.44
8	Max. Patch Area	log(y) ~ log(x)	0.82
9	Mean Shape Index	log(y) ~ log(x)	0.06
10	Std. Dev. of Shape Index	y ~ log(x)	0.36
12	Max. Shape Index	log(y) ~ log(x)	0.83
13	Proportion of Like Adjacencies	y ~ log(x)	0.12
14	Patch Cohesion Index	log(y) ~ log(x)	0.54

Table 1.4: Best fit models for metric by dominant length scale

models to use in the subsequent analysis. This allowed comparison of metric values across scales by removing the scaling effects on the metric values of increasing the calculation extent. From now on when referring to metric values we are referring to the metric values detrended for extent unless otherwise specified. By using the residuals from the regression models, we remove the effects of the variable resolution of the extents while still preserving the relationship between LST and the metric value because the metrics were calculated within areas determined by the dominant length scale of vegetation-LST interaction.

All landscape metrics were significantly correlated with the percent vegetation (Table 1.3). Following the work of Hu & Brunsell (2015), the observations were classified into ten equal-interval classes representing the percent vegetated surface within each extent to isolate the effects of landscape composition on the UHI. We then plotted the landscape metrics against LST by percent vegetated class to examine the effects of greenspace configuration on the UHI while controlling for vegetation composition.

1.4.2 Landscape metrics and LST

The calculated landscape metrics represent landscape pattern within an extent defined by the characteristic scale of LST-vegetation interactions. This analysis seeks to identify how LST varies in

	Metric (Scale Resid.)	Metric
Patch Density	0.06***	0.03
Total Edge	-0.16***	0.02
Edge Density	-0.2***	-0.2***
Largest Patch Index	-0.34***	-0.31***
Mean Patch Area	-0.34***	-0.13***
Std. Dev. of Patch Area	-0.31***	-0.14***
Max. Patch Area	-0.34***	-0.08***
Mean Shape Index	-0.09***	-0.09***
Std. Dev. of Shape Index	-0.21***	-0.14***
Max. Shape Index	-0.04*	0
Proportion of Like Adjacencies	-0.29***	-0.25***
Patch Cohesion Index	-0.19***	-0.08***
Percent Vegetated	-0.19***	-0.08***

Table 1.5: Pearson correlation coefficients for metrics and LST, including percent vegetated. The values on the left are modeled on the metric value after scale effects were removed. The values on the right are modeled on the uncorrected metric values. $p < .001$ ***, $p < .01$ **, $p < .05$ *

relationship to pattern. To do so we assessed the way LST is higher or lower than the median for that day and how that varies with landscape pattern. We developed a Pearson correlation matrix to assess the strength of the relationships between LST and the independent variables of composition and configuration of greenspace. We then used linear regression models to further examine the relationships between metrics and LST. A model was fit between each metric and LST for all vegetated classes and also within each vegetated class.

The Pearson correlation coefficients show that all metrics are significantly correlated with LST (Table 1.5). They also show that removing the scale effects from the metric values improved all models except edge density and mean shape index which remained the same. All relationships are negative (as the metric value increases, LST decreases relative to the median) except for patch density. It is interesting to note that percent vegetated has a weaker correlation with LST than several other metrics. However, all the metrics except for total edge and edge density are also significantly correlated with percent vegetated (Table 1.3).

In order to more fully understand the relationship between greenspace configuration and LST while controlling for the percent of vegetation, we constructed a Pearson correlation matrix for LST and each metric by percent vegetated class. The correlation between mean patch area, maxi-

mum patch area, the standard deviation of patch area, and the largest patch index and LST increase as percent vegetated class increases, indicating that their affect on LST is primarily due to composition. The correlations between mean shape index, maximum shape index, and the standard deviation of shape index and LST are not consistently significant across the percent vegetated classes, indicating that there is not a strong relationship. Proportion of like adjacencies and patch cohesion index have positive and significant correlations with LST for 30 - 70% vegetated areas (although proportion of like adjacencies is not significantly correlated with LST for 30 - 40% vegetated areas), indicating that in moderately vegetated areas dispersed rather than clustered green space more effectively lowers LST. Patch density has significant and negative correlations with LST for areas with 20 - 80% vegetated area, indicating that given a certain amount of greenspace, more small patches more effectively mitigates UHIs than fewer large patches. Edge density and total edge also have highly significant and negative correlations with LST for areas with more than 40% vegetated area, indicating that complex shapes more effectively lower LST (Fig. 1.8).

Linear models were developed for LST against each metric, and the R^2 value, significance, and slope calculated for the model applied at each percent vegetated class (Fig. 1.9). When considered across all vegetated classes, all metrics have a significant relationship with LST, however, when considered within each vegetated class many of these relationships break down. This highlights the importance of controlling for the percent vegetated when examining landscape configuration. It is important to note that many of the relationships between the landscape metrics and LST change direction across vegetated classes. For instance, while the slope for the overall relationship between patch density and LST is significant and positive, the relationship is significant and negative for 20 - 80% vegetated areas. Standard deviation of patch area, proportion of like adjacencies, patch density, patch cohesion index, mean patch area, maximum patch area, and largest patch index all exhibit this behavior. The relationships between standard deviation, mean, and maximum shape index and LST change direction in unpredictable ways. The relationships between total edge and edge density and LST are negative for areas with greater than 20% vegetated area (Table 1.3).

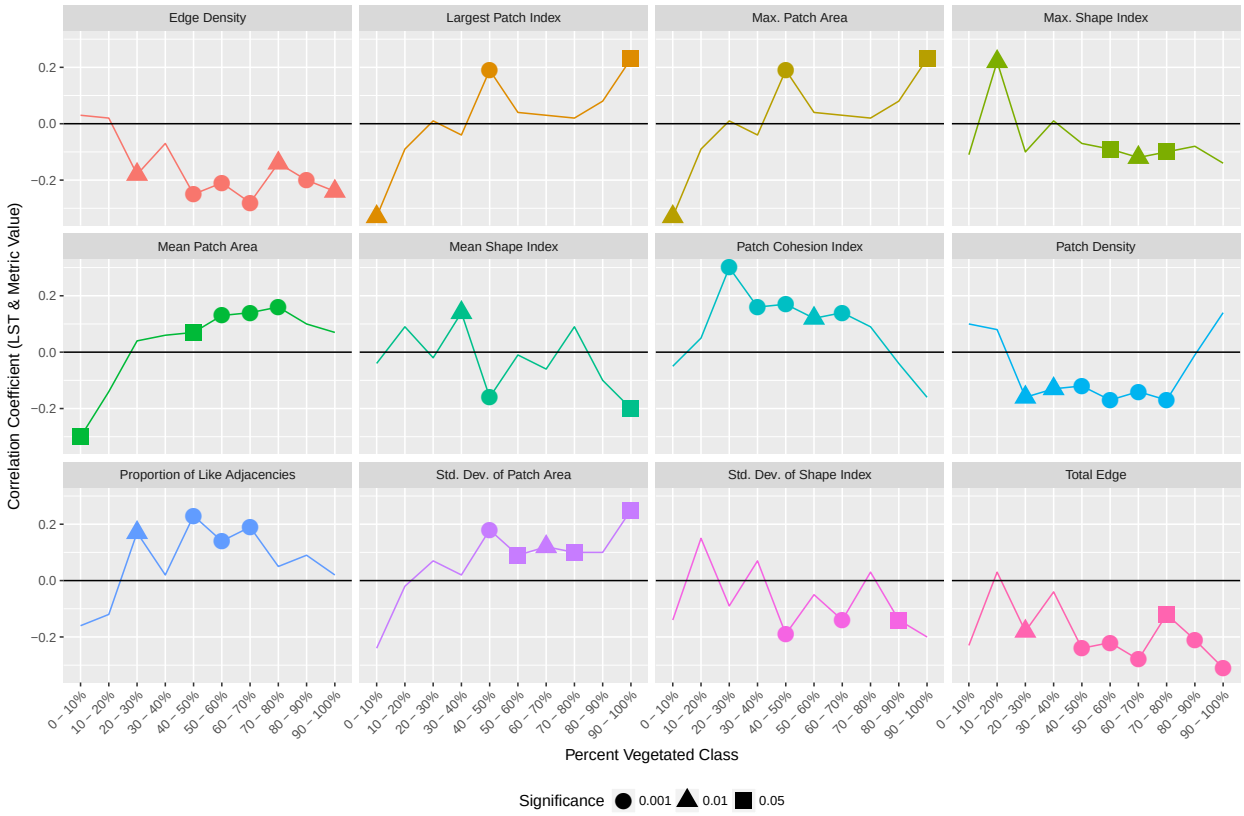

Figure 1.8: Variation of correlation coefficients for LST and metrics across percent vegetated classes.

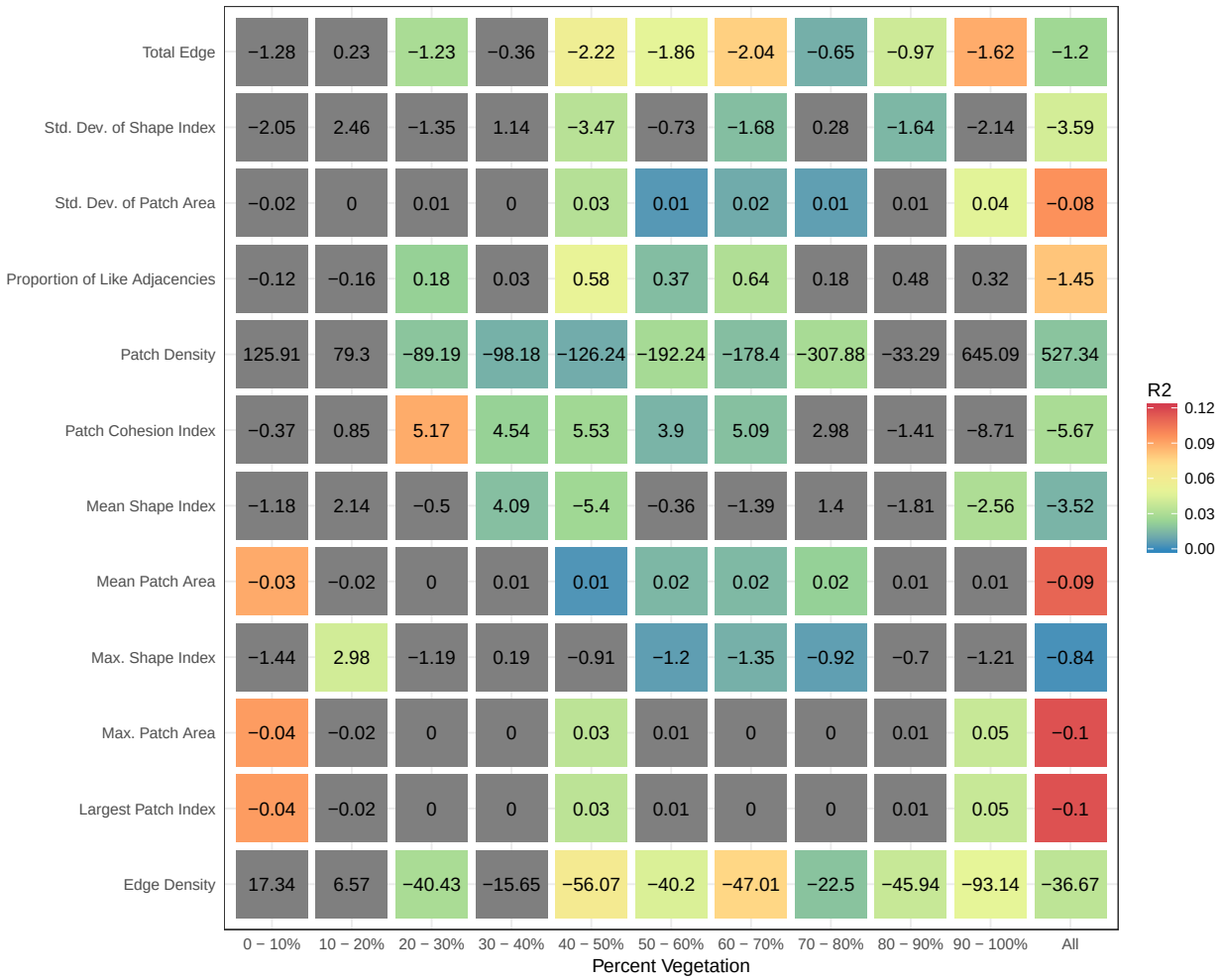

Figure 1.9: Linear regression of LST by metric value across percent vegetated classes. The numbers are the slope of the relationship and grid cells in grey indicate models not significant at the 0.05 level.

1.5 Discussion

In this study we used the dominant length scales of vegetation-LST interaction as extents to calculate landscape metrics in order to examine the relationship between landscape pattern and the UHI in the Kansas City metropolitan area. Due to the the complex nature of urban areas, the nature of landscape metric calculations, and the variability of local climate it can be difficult to discern real relationships from spurious effects (Kim & Baik, 2005; Weng et al., 2008; Grafius et al., 2018). To ensure robust results, we analyzed LST from six dates, calculated landscape metrics within biophysically determined extents, removed the trends from increasing calculation extent from the landscape metric values, and controlled for the percent vegetated. Although the overall explanatory power of the individual metrics with regard to LST is relatively low after removing the effects of the percent of vegetation ($R^2 < 0.10$), there remain significant relationships between greenspace pattern and LST.

Similar to Maimaitiyiming et al. (2014) and Zhou et al. (2011) we found that increasing edge density can lower LSTs. This increase in edge density produces more complex shapes and may enhance the interactions between vegetated and non-vegetated surfaces and facilitate energy exchange (Zhou et al., 2011). Also in agreement with Zhou et al. (2011) and Stone & Rodgers (2001), our results show that dispersed rather than clustered greenspace more effectively mitigates UHIs. Increased patch density lowers LST while increased patch cohesion index (a measure of aggregation) increases LST.

Our findings that the overall negative relationship between patch size and LST is an artifact of the correlation between patch size and percent vegetation are supported by Zhou et al. (2011). In fact, our results show that while the overall relationship between mean patch size and LST is negative, for 40 - 80% vegetated areas the relationship is positive, meaning that an increase in mean patch size actually increases LST. As the mean patch size increases in areas in the mid-vegetated classes, aggregation of greenspace would likely increase; our results show that aggregation increases LST. These results contradict findings by Li et al. (2012) who found a significant negative relationship between mean patch size and LST. However, their study used census tracts as the ana-

lytical unit because they are the level of local urban planning in the study area. It is our contention that pattern analysis should take place at the characteristic scale of vegetation-LST interaction and that comparing pattern in variably sized extents that are not biophysically relevant fails to capture the complexity of urban energy interactions (Wu, 2007; Weng et al., 2008).

Results from this study can be used to guide urban planners in designing and manipulating the urban environment. Planting street trees, increasing urban vegetation, and greenspace management can be optimized to provide maximum UHI mitigation and land-use zoning is a powerful tool for urban planners to impact the thermal conditions of urban landscapes (Weng et al., 2007). Especially in periurban areas, development can be regulated to minimize the negative effects of replacing vegetated with impervious surfaces. While we found that increasing edge density and patch density may effectively lower LSTs in the Kansas City metropolitan area, it is important to note that a much greater percent of LST variability is explained by the percent vegetated. Given a set amount of greenspace, the configuration can be optimized for UHI mitigation, but more importantly, increasing the amount of vegetation will always have a positive effect on LST (Buyantuyev & Wu, 2007; Li et al., 2011; Maimaitiyiming et al., 2014).

This study only analyzed the UHI of one region. While the results of this study may be broadly applicable in other urbanized areas it is possible that the unique characteristics of the Kansas City metropolitan area may affect the relationship between LST and greenspace pattern in a singular way. Further research should extend these methods to other urban areas with different morphologies in different climate zones.

1.6 Conclusion

By using the dominant length scales of LST we not only demonstrate that aggregation and shape complexity are important configuration factors to consider in designing urban greenspace, we also provide a methodology for robust biophysically-based analysis of urban landscape pattern. As global urban population increases, understanding urban energy dynamics will be increasingly important for ensuring the health and well being of societies. Urban greenspace provides multiple

ecosystem services including stormwater runoff control, habitat provision, psychological benefits, and LST reduction. By designing urban areas to include more and complex patches of greenspace, urban planners can effectively mitigate UHIs.

References

Akbari, H., Pomerantz, M., & Taha, H. (2001). Cool surfaces and shade trees to reduce energy use and improve air quality in urban areas. *Solar Energy*, 70(3), 295–310.

Alberti, M. (2010). Maintaining ecological integrity and sustaining ecosystem function in urban areas. *Current Opinion in Environmental Sustainability*, 2(3), 178–184.

Brunsell, N. A. & Gillies, R. R. (2002). Incorporating surface emissivity into a thermal atmospheric correction. *Photogrammetric Engineering and Remote Sensing*, 68(12), 1263–1269.

Brunsell, N. A. & Gillies, R. R. (2003). Length Scale Analysis of Surface Energy Fluxes Derived from Remote Sensing. *Journal of Hydrometeorology*, 4(6), 1212–1219.

Buyantuyev, A. & Wu, J. (2007). Effects of thematic resolution on landscape pattern analysis. *Landscape Ecology*, 22(1), 7–13.

Buyantuyev, A. & Wu, J. (2010). Urban heat islands and landscape heterogeneity: Linking spatiotemporal variations in surface temperatures to land-cover and socioeconomic patterns. *Landscape Ecology*, 25(1), 17–33.

Buyantuyev, A., Wu, J., & Gries, C. (2010). Multiscale analysis of the urbanization pattern of the Phoenix metropolitan landscape of USA: Time, space and thematic resolution. *Landscape and Urban Planning*, 94(3-4), 206–217.

Chen, Y. & Yu, S. (2017). Impacts of urban landscape patterns on urban thermal variations in Guangzhou, China. *International Journal of Applied Earth Observation and Geoinformation*, 54, 65–71.

Estoque, R. C., Murayama, Y., & Myint, S. W. (2017). Effects of landscape composition and pattern on land surface temperature: An urban heat island study in the megacities of Southeast Asia. *Science of the Total Environment*, 577, 349–359.

Evans, J. S. (2017). spatialEco.

Gillies, R. R. & Carlson, T. N. (1995). Thermal Remote Sensing of Surface Soil Water Content with Partial Vegetation Cover for Incorporation into Climate Models. *Journal of Applied Meteorology*, 34(4), 745–756.

Grafius, D. R., Corstanje, R., & Harris, J. A. (2018). Linking ecosystem services, urban form and green space configuration using multivariate landscape metric analysis. *Landscape Ecology*, 33(4), 1–17.

Grimmond, C. S. B. & Oke, T. R. (1991). An Evapotranspiration-Interception Model for Urban Areas. *Water Resources Research*, 27(7), 1739–1755.

Güneralp, B., Zhou, Y., Ürge-Vorsatz, D., Gupta, M., Yu, S., Patel, P. L., Fragkias, M., Li, X., & Seto, K. C. (2017). Global scenarios of urban density and its impacts on building energy use through 2050. *Proceedings of the National Academy of Sciences*, 114(34), 201606035.

Hu, L. & Brunsell, N. A. (2015). A new perspective to assess the urban heat island through remotely sensed atmospheric profiles. *Remote Sensing of Environment*, 158, 393–406.

Huang, G., Zhou, W., & Cadenasso, M. L. (2011). Is everyone hot in the city? Spatial pattern of land surface temperatures, land cover and neighborhood socioeconomic characteristics in Baltimore, MD. *Journal of Environmental Management*, 92(7), 1753–1759.

Imhoff, M. L., Zhang, P., Wolfe, R. E., & Bounoua, L. (2010). Remote sensing of the urban heat island effect across biomes in the continental USA. *Remote Sensing of Environment*, 114(3), 504–513.

IPCC (2014). *Climate Change 2014: Synthesis Report. Contribution of Working Groups I, II and III to the Fifth Assessment Report of the Intergovernmental Panel on Climate Change*. Technical report.

Ji, W. (2008). Landscape effects of urban sprawl: Spatial and temporal analyses using remote sensing images and landscape metrics. *The International Archives of the Photogrammetry, Remote Sensing and Spatial Information Sciences*, XXXVII(B7), 1691–1694.

Kim, Y. H. & Baik, J.-J. (2005). Spatial and temporal structure of the urban heat island in Seoul. *Journal of Applied Meteorology*, 44(5), 591–605.

Kumar, P. & Foufoula-Georgiou, E. (1997). Wavelet Analysis for Geophysical Applications. *Reviews of Geophysics*, 35(4), 385–412.

Leitao, A. B. & Ahern, J. (2002). Applying landscape ecological concepts and metrics in sustainable landscape planning. *Landscape and Urban Planning*, 59(2), 65–93.

Li, J., Song, C., Cao, L., Zhu, F., Meng, X., & Wu, J. (2011). Impacts of landscape structure on surface urban heat islands: A case study of Shanghai, China. *Remote Sensing of Environment*, 115(12), 3249–3263.

Li, X., Li, W., Middel, A., Harlan, S. L., Brazel, A. J., & Turner, B. L. (2016). Remote sensing of the surface urban heat island and land architecture in Phoenix, Arizona: Combined effects of land composition and configuration and cadastral-demographic-economic factors. *Remote Sensing of Environment*, 174, 233–243.

Li, X., Zhou, W., & Ouyang, Z. (2013). Relationship between land surface temperature and spatial pattern of greenspace: What are the effects of spatial resolution? *Landscape and Urban Planning*, 114, 1–8.

Li, X., Zhou, W., Ouyang, Z., Xu, W., & Zheng, H. (2012). Spatial pattern of greenspace af-

fects land surface temperature: Evidence from the heavily urbanized Beijing metropolitan area, China. *Landscape Ecology*, 27(6), 887–898.

Liu, H. & Weng, Q. (2009). Scaling Effect on the Relationship between Landscape Pattern and Land Surface Temperature: A Case Study of Indianapolis, United States. *Photogrammetric Engineering and Remote Sensing*, 75(3), 291–304.

Luber, G. & McGeehin, M. (2008). Climate Change and Extreme Heat Events. *American Journal of Preventive Medicine*, 35(5), 429–435.

Maimaitiyiming, M., Ghulam, A., Tiyip, T., Pla, F., Latorre-Carmona, P., Halik, Ü., Sawut, M., & Caetano, M. (2014). Effects of green space spatial pattern on land surface temperature: Implications for sustainable urban planning and climate change adaptation. *ISPRS Journal of Photogrammetry and Remote Sensing*, 89, 59–66.

McGarigal, K. (2014). FRAGSTATS help.

Meehl, G. A. & Tebaldi, C. (2004). More intense, more frequent, and longer lasting heat waves in the 21st century. *Science*, 305, 994–7.

Mid-America Regional Council (2013). Kansas City Natural Resource Inventory II: Beyond the Map Summary Report.

Oke, T. R. (1995). The heat island of the urban boundary layer: characteristics, causes and effects. In *Wind climate in cities* (pp. 81–107). Springer.

Patz, J. A., Campbell-Lendrum, D., Holloway, T., & Foley, J. A. (2005). Impact of regional climate change on human health. *Nature*, 438(7066), 310–317.

Stone, B., Hess, J. J., & Frumkin, H. (2010). Urban form and extreme heat events: Are sprawling cities more vulnerable to climate change than compact cities? *Environmental Health Perspectives*, 118(10), 1425–1428.

Stone, B. & Norman, J. M. (2006). Land use planning and surface heat island formation: A parcel-based radiation flux approach. *Atmospheric Environment*, 40(19), 3561–3573.

Stone, B. & Rodgers, M. O. (2001). Urban Form and Thermal Efficiency: How the Design of Cities Influences the Urban Heat Island Effect. *Journal of the American Planning Association*, 67(2), 186–198.

Stone, B., Vargo, J., & Habeeb, D. (2012). Managing climate change in cities: Will climate action plans work? *Landscape and Urban Planning*, 107(3), 263–271.

Stott, P. A., Stone, D. A., & Allen, M. R. (2004). Human contribution to the European heatwave of 2003. *Nature*, 432(7017), 610–613.

Streutker, D. R. (2002). A remote sensing study of the urban heat island of Houston, Texas. *International Journal of Remote Sensing*, 23(13), 2595–2608.

Synnefa, A., Santamouris, M., & Akbari, H. (2007). Estimating the effect of using cool coatings on energy loads and thermal comfort in residential buildings in various climatic conditions. *Energy and Buildings*, 39, 1167–1174.

United Nations (2014). *World Urbanization Prospects 2014*. Technical report.

U.S. Geological Survey (2016). Landsat 8 (L8) Data Users Handbook.

Van de Voorde, T., Jacquet, W., & Canters, F. (2011). Mapping form and function in urban areas: An approach based on urban metrics and continuous impervious surface data. *Landscape and Urban Planning*, 102(3), 143–155.

Voogt, J. A. & Oke, T. R. (2003). Thermal remote sensing of urban climates. *Remote Sensing of Environment*, 86(3), 370–384.

Weng, Q., Liu, H., & Lu, D. (2007). Assessing the effects of land use and land cover patterns on thermal conditions using landscape metrics in city of Indianapolis, United States. *Urban Ecosystems*, 10(2), 203–219.

Weng, Q., Lu, D., & Schubring, J. (2004). Estimation of land surface temperature-vegetation abundance relationship for urban heat island studies. *Remote Sensing of Environment*, 89(4), 467–483.

Weng, Q. H., Liu, H., Liang, B. Q., & Lu, D. S. (2008). The Spatial Variations of Urban Land Surface Temperatures: Pertinent Factors, Zoning Effect, and Seasonal Variability. *Ieee Journal of Selected Topics in Applied Earth Observations and Remote Sensing*, 1(2), 154–166.

Whitcher, B. (2014). Package 'waveslim'.

Wu, J. (2004). Effects of changing scale on landscape pattern analysis : scaling relations. *Landscape Ecol Eng*, 19, 125–138.

Wu, J. (2007). Scale and scaling: a cross-disciplinary perspective. *Key topics in landscape ecology*, (January 2007), 115 – 136.

Wu, J. (2010). Urban sustainability: An inevitable goal of landscape research. *Landscape Ecology*, 25(1), 1–4.

Xu, H. (2006). Modification of normalised difference water index (NDWI) to enhance open water features in remotely sensed imagery. *International Journal of Remote Sensing*, 27(14), 3025–3033.

Yuan, F. & Bauer, M. E. (2007). Comparison of impervious surface area and normalized difference vegetation index as indicators of surface urban heat island effects in Landsat imagery. *Remote Sensing of Environment*, 106(3), 375–386.

Zhou, W., Huang, G., & Cadenasso, M. L. (2011). Does spatial configuration matter? Understanding the effects of land cover pattern on land surface temperature in urban landscapes. *Landscape and Urban Planning*, 102, 54–63.

Zhou, Y., Smith, S. J., Elvidge, C. D., Zhao, K., Thomson, A., & Imhoff, M. (2014). A cluster-based method to map urban area from DMSP/OLS nightlights. *Remote Sensing of Environment*, 147, 173–185.